

Monte Carlo simulation of positron-stimulated secondary electron emission from solids

Maurizio Dapor

Istituto Trentino di Cultura and Istituto Nazionale per la Fisica della Materia, I-38050 Povo, Trento, Italy

Antonio Miotello

Istituto Nazionale per la Fisica della Materia and Dipartimento di Fisica dell'Università di Trento, I-38050 Povo, Trento, Italy

Davide Zari

Istituto Trentino di Cultura and Dipartimento di Fisica dell'Università di Trento, I-38050 Povo, Trento, Italy

(Received 8 June 1999; revised manuscript received 1 October 1999)

We have analyzed the problem of the secondary electrons emitted from a solid irradiated by a positron or electron particle beam. The relevant concepts that form the basis for a theoretical understanding of the secondary electron emission problem are reanalyzed by looking at Wolff's theory. However, to attain analytical results, such a theory must include some simplification, which may be valid in only a limited number of situations. To overcome such a limitation we have elaborated a Monte Carlo procedure for the calculation of the secondary electrons emitted from a solid, irradiated with a positron beam. The choice of a primary positron beam is justified because the experiments involving electron emission are not contaminated by the reemitted primary electrons. The calculations were performed in the positron primary energy range between 50 eV and 2 keV, and for different incidence angles with respect to the surface of a copper sample. Many numerical results are reported, namely: i) the elastic mean-free paths of positrons in copper, ii) the mean number of electrons emitted per positron, iii) the penetration depth of the positrons, and iv) the depths from which the secondary electrons are emitted. Finally, the numerical results concerning the secondary electron energy distribution are compared with the experimental data recently presented by Overton and Coleman showing a general good agreement.

I. INTRODUCTION

The problem of secondary electron emission from solids irradiated by a particle beam is relevant, mainly in connection with the analytical techniques that utilize secondary electrons to investigate chemical and compositional properties of solids in the near surface layers: Auger electron spectroscopy and X-photoelectron spectroscopy. In general, the energy spectra of the emitted electrons are quite complicated because many features appear in such a spectra in connection with the different collisional processes involved before low-energy secondary electron emission. As a consequence, a better understanding of the collisional events occurring in the surface layers before emission, should permit a more general understanding of the surface physics including, for example, plasmon excitation. Recently, the collisional processes of positron beams impinging on solids received great attention because of the possibility to realize, by positron annihilation spectroscopy, nondestructive investigations of point and extended defects of surfaces, interfaces, and of bulk materials. Review papers on the subject have been prepared by Dupasquier and Zecca,¹ Schultz and Lynn,² and Asoka-Kumar *et al.*³

When a particle beam, with particle energy exceeding some threshold value, impinges on a solid target, it stimulates the emission of secondary electrons through collisions with target atoms. On the other hand, a fraction of the particles of the primary beam is also ejected from the surface because, after a number of elastic and/or inelastic collisions with the target atoms, some of those particles come back and

emerge from the surface. If the target is not a thin film (namely, if there are not transmitted particles) the remaining primary particles are trapped into it. For bulk targets the ratio between the number of backscattered and total (backscattered+trapped) particles is generally called the backscattering coefficient.

If the primary particles are electrons, then the spectrum of the secondary electrons is clearly contaminated by the contribution of the backscattered primary electrons. On the other hand, as recently noted by Overton and Coleman,⁴ the problem of distinguishing between true secondary and backscattered electrons is absent, if the secondary electron emission is stimulated by positron beams. In the quoted paper,⁴ the authors performed an interesting experimental study of the spectra of fast secondary electrons not contaminated by the backscattered electrons. Specifically, secondary electrons produced by positron beams, impinging on copper target at glancing and 35° incidence angle and for primary energies in the range from 50 eV to 2 keV, have been analyzed.⁴

Experimental results have been compared to the Sickafus⁵⁻⁷ empirical law:

$$j(E) = AE^{-m}, \quad (1)$$

where $j(E)$ represents the measured secondary electron energy distribution, E being the energy of the emitted secondary electrons, while A and m are constants that depend on the solid and on the energy of the impinging positrons.

The comparison shows excellent linear correlation when

the data are plotted as $\log_{10}[j(E)]$ vs $\log_{10}(E)$ and the values of m are reported as a function of the energy of the colliding positrons.

In the present paper, we try to explain the experimental results⁴ by using a Monte Carlo code in which, essentially, the positron-solid interaction is included as described by the relevant cross sections and stopping-powers of the collisional processes (both elastic and inelastic) and the corresponding mean-free paths.

However, before to illustrate the numerical procedure we have adopted, it is important to gain some insights into the relation (1) by looking at the previously proposed analytical models. In this way, we will understand the theoretical framework that forms the basis to approach the problem of the secondary electron emission as well as the limits of the analytical procedures, which, on the contrary, may be overcome by numerical methods, mainly based on a Monte Carlo simulation. Let us now reanalyze Wolff's theory⁸ to underline the basic concepts necessary to analyze the secondary electron emission problem.

II. ANALYTICAL CONCEPTS RELATED TO THE SECONDARY ELECTRON EMISSION

The secondary electrons production occurs in two steps. The first step is the secondary electrons production due to the impacts between the primaries particles and the electrons bound in the solid. The second process is the so-called cascade: the secondary electrons travel in the material producing other secondaries before being trapped in the solid or before emerging from the surface. The equations that govern the cascade process, as deduced from the Boltzmann transport equation, for the steady state, when the primary particles collide normally with the target surface in the z direction, are the following:⁸

$$\psi_l = \lambda(E) \left[\frac{l}{2l+1} \frac{\partial \psi_{l-1}}{\partial z} + \frac{l+1}{2l+1} \frac{\partial \psi_{l+1}}{\partial z} \right] + \int_E^\infty dE' F_l(E, E') \psi_l(z, E') + S_l(z, E). \quad (2)$$

In this set of integro-differential equations,

$$\psi_l = v N_l / \lambda(E), \quad (3)$$

$\lambda(E)$ is the electron mean-free path, v is the electron velocity, E is the electron energy, and N_l , F_l , and S_l are the coefficients of the following expansions in spherical harmonics:

$$N(z, \cos \theta, E) = \frac{1}{4\pi} \sum_{l=0}^{\infty} (2l+1) N_l(z, E) P_l(\cos \theta), \quad (4)$$

$$S(z, \cos \theta, E) = \frac{1}{4\pi} \sum_{l=0}^{\infty} (2l+1) S_l(z, E) P_l(\cos \theta), \quad (5)$$

$$F(\mathbf{\Omega}, E; \mathbf{\Omega}', E') = F(\cos \Theta; E, E') = \frac{1}{4\pi} \sum_{l=0}^{\infty} (2l+1) F_l(E, E') P_l(\cos \Theta). \quad (6)$$

Here N is the number of electrons between \mathbf{r} and $\mathbf{r} + d\mathbf{r}$, $\mathbf{\Omega}$ and $\mathbf{\Omega} + d\mathbf{\Omega}$, E and $E + dE$. $\mathbf{\Omega}$ is a unit vector in the velocity direction, S is a source term that represents the secondary electrons produced by the primary beam, and F is the probability that, given an electron at $\mathbf{\Omega}'$ with energy E' , another electron will be found after scattering at $\mathbf{\Omega}$ with energy E . Θ is the angle between the directions $\mathbf{\Omega}$ and $\mathbf{\Omega}'$. P_l are the Legendres's polynomials.

It is evident that the set of equations (2) is quite complicated to be utilized and an approximate approach is needed. In particular, Wolff⁸ observed that the high- l harmonics become important only for high energies. For low energies ψ_0 overwhelms the other harmonics because it grows rapidly as $E \rightarrow 0$. In this case

$$j(E) = \psi_0 \lambda(E). \quad (7)$$

By utilizing the Goldberger's evaluation of the probability of scattering from E' to E (for S -wave scattering from a degenerate Fermi gas)⁹ and taking into account the exclusion principle, Wolff showed that⁸

$$\psi_0 \propto \left(\frac{E_o}{E} \right)^{x(E)}, \quad (8)$$

where $x(E)$ decreases as energy increases from E_f to $\sim 4E_f$ and equals 2 for energies higher than $\sim 4E_f$ (E_f is the Fermi energy). For $E \rightarrow 2E_f$, $x(E) \rightarrow 2.3$. E_o is the primary particle-beam energy. The proportionality constant, in Eq. (8), that we will indicate as $P(E)$, is a geometrical factor representing the probability that an electron reaching the surface have a large enough normal velocity component to escape. Assuming a spherical symmetric distribution and indicating with φ the work function, $P(E)$ can be calculated through

$$P(E) = 1 - \sqrt{\frac{\varphi + E_f}{E}}. \quad (9)$$

The Goldberger's evaluation of the reduction of the total scattering cross-section due to the exclusion principle entails the following equation for the mean-free path (valid for $E > 2E_f$)

$$\lambda(E) = \frac{1}{n_c \sigma_{inel}(E) (1 - 7E_f/5E)}, \quad (10)$$

where n_c is the number density of conduction band electrons, and $\sigma_{inel}(E)$ is the electron-electron inelastic scattering cross section. By utilizing Eqs. (7)–(10), Wolff's formula follows:

$$j(E) = \frac{1 - \sqrt{(\varphi + E_f)/E}}{n_c \sigma_{inel}(E) (1 - 7E_f/5E)} \left(\frac{E_o}{E} \right)^{x(E)}. \quad (11)$$

III. APPROXIMATE ANALYTICAL RELATIONS FOR PRIMARY ELECTRON ENERGY EXCEEDING 100 eV

Wolff's theory, in the approximation represented by Eq. (11), gives the spectrum of the secondary electrons when the primary electron or positron energy is less than $W = 100$ eV: indeed for energies lower than W electron-electron and positron-electron scattering processes can be as-

sumed to be spherically symmetric. Since the shapes of the secondary electron spectra, on the other hand, are substantially determined by electrons with energies lower than 40 eV, the spectra are quite insensitive to the choice of W .⁸

Sickafus⁵ empirically tried to extend the energy range of Wolff's cascade theory. He assumed that $E \gg E_f$ and observed that, in such a case, $P(E) \sim 1$, $(1 - 7E_f/5E) \sim 1$, and $x(E) \sim 2$. As a consequence

$$j(E) \propto \frac{E_o^x}{\sigma_{inel}(E)E^x}. \quad (12)$$

Assuming that the inelastic cross section has the following form:¹⁰

$$\sigma_{inel} \propto \frac{\log E}{E}, \quad (13)$$

then

$$j(E) = C \frac{E_o^x}{E^{x-1} \log E}, \quad (14)$$

where C is a constant. As a consequence,

$$\log j(E) = x \log E_o - (x-1) \log E - \log \log E + \log C. \quad (15)$$

Since the function $\log \log E$ is almost constant, on a given range of E , we conclude that, for any given primary energy E_o , $\log j(E)$ as a function of $\log E$ is given by

$$\log j(E) = k - m \log E. \quad (16)$$

where $m \sim 1$ and k is a constant.

In other words, a plot of $\log j(E)$ versus $\log E$ presents a linear trend (the so-called Sickafus region of the spectrum) and the value of m should be approximately 1.

On the other hand, by utilizing the dielectric function approach¹¹⁻¹³ to calculate the inelastic cross section, and by empirically introducing the results directly into the Wolff formula [Eq. (11)], we obtained, for primary energies lower than 1000 eV, spectra with values of m higher than ~ 2 . In particular, for copper, we found that $m = 2.24 \pm 0.04$ and $m = 2.01 \pm 0.04$ when E_o is equal to 500 and 1000 eV, respectively. Note that the interval regions where the slopes of the log-log plots have been calculated were quite restricted, being 50–155 eV for $E_o = 500$ eV, and 50–270 eV for $E_o = 1000$ eV, while the corresponding linear correlations coefficients were, respectively, 0.997 and 0.995.

Wolff's theory give results that are surprisingly good, if compared with many experimental data, even if these data are outside the claimed limits of validity of the theory. It is reasonable to conclude that Wolff's theory could be extended outside the ~ 100 eV because the shapes of the secondary electrons spectra are dominated by the low-energy electrons.

However, in order to avoid empirical procedures to obtain m , and to include also the elastic scattering collisions, we decided to simulate the positron and the electron trajectories with a Monte Carlo procedure based on the dielectric

function approach for inelastic scattering and on the Relativistic Partial Wave Expansion Method (RPWEM) for elastic scattering.

IV. THE MONTE CARLO SCHEME

The Monte Carlo method is a very powerful and reliable procedure to evaluate important quantities related to the electron-solid and positron-solid interaction, such as backscattering coefficients and implantation profiles,^{14,16,17,15} secondary electron emission,^{18,19} and spectra of backscattered and of secondary electrons.^{20,21} In the present calculation, the elastic scattering of both positrons and secondary electrons is computed step by step along the path of the particle by cubic spline interpolation of extensive tabulations of the differential elastic scattering cross section obtained by the code we described elsewhere.^{22,23} The use of cubic spline interpolation rather than direct calculation is due to the fact that the direct computation of the differential scattering cross sections requires a large amount of computational time. Any way, the adopted Monte Carlo scheme is very accurate in the determination of the scattering angle, θ , after every elastic collision (errors being within 1–5 %).²³

Concerning the inelastic scattering, we have used the Ashley treatment^{11,13} for the calculation of the stopping power, dE/ds , and inelastic mean-free path, λ_{inel} . Our calculations are in excellent agreement with those of Ashley.^{11,13} In order to expedite the computer simulation we also have used a cubic spline interpolation of previously computed and tabulated data for inelastic scattering, as for the elastic case. Before each step of the particle trajectory, a random number, uniformly distributed in the range [0,1], is generated and compared to the probability of inelastic scattering. If the random number is lower than that probability, then the collision will be inelastic. The probability of inelastic scattering p_{inel} is given by

$$p_{inel} = \lambda_{inel}^{-1} / (\lambda_{inel}^{-1} + \lambda_{el}^{-1}). \quad (17)$$

In this equation, λ_{el} and λ_{inel} are, respectively, the elastic and the inelastic mean-free paths:

$$\lambda_{el} = \frac{1}{\mathcal{N}\sigma_{el}}, \quad (18)$$

$$\lambda_{inel} = \frac{1}{\mathcal{N}\sigma_{inel}}, \quad (19)$$

where σ_{el} is the total elastic scattering cross section, σ_{inel} is the total inelastic scattering cross section, and \mathcal{N} is the number of atoms per unit of volume in the target.

The step-length, Δs , is calculated as

$$\Delta s = -\lambda_{tot} \cdot \ln(r_{\Delta s}), \quad (20)$$

where $r_{\Delta s}$ is a random number uniformly distributed in the range [0,1] and λ_{tot} is defined by

$$\lambda_{tot}^{-1} = \lambda_{inel}^{-1} + \lambda_{el}^{-1}. \quad (21)$$

If the collision is elastic, then we assume that the incident particle changes its direction in agreement with the differential elastic scattering cross section obtained by the RPWEM.^{22,23}

The polar scattering angle, θ , after an elastic collision is selected via a random number, r_θ , uniformly distributed in the range $[0,1]$. The choice is such that the integrated probability for scattering in the angular range from 0 to θ equals r_θ :

$$r_\theta = \frac{2\pi \int_0^\theta \frac{d\sigma}{d\Omega} \sin \vartheta d\vartheta}{2\pi \int_0^\pi \frac{d\sigma}{d\Omega} \sin \vartheta d\vartheta}. \quad (22)$$

If the collision is inelastic, the energy loss can be evaluated by utilizing a random number $r_{\Delta E}$, uniformly distributed in the range $[0,1]$ so that

$$r_{\Delta E} = \frac{\int_0^{\Delta E} (d\lambda_{inel}^{-1}/dT) dT}{\int_0^{E-E_f} (d\lambda_{inel}^{-1}/dT) dT}, \quad (23)$$

where $(d\lambda_{inel}^{-1}/dT)$ represents the probability for energy loss T per unit distance travelled by an electron of energy E , i.e., the inverse mean-free path differential in energy transfer.

This process of evaluation of the energy loss is quite time consuming. Then, in order to expedite the calculations, we introduced the following approximation. Along each step Δs of the particle trajectory we approximated the energy losses assuming that the particle loses an amount of energy, which is evaluated by multiplying the stopping power, dE/ds , by the step-length Δs , namely:

$$\Delta E = \frac{dE}{ds} \Delta s. \quad (24)$$

Actually the use of the stopping power within the continuous energy loss approximation for the evaluation of the energy loss is a rough simplification: positrons and electrons can lose, indeed, large amounts of their energy in single collisions. So, in order to check the validity of the present numerical procedure in relation to the whole energy loss of the positrons penetrating into a solid, we compared our calculated maximum range with the data of Mills and Wilson concerning the transmission of 1–6 keV positrons through thin metal films.²⁴ These authors evaluated with great accuracy the maximum range of keV-positrons in Al and in Cu: for 3100 eV positrons in Cu they found an experimental range equal to 69.1 nm while with our numerical code we obtained, in the same conditions adopted in the experiments,²⁴ a range of 70.8 ± 0.7 nm. The comparison with other energies may be found in Table IV that we will comment below.

The polar scattering angle, θ , after each inelastic collision is calculated as

$$\sin \theta = \sqrt{\frac{\Delta E}{E}}. \quad (25)$$

The azimuthal angle ϕ after each collision (elastic or inelastic) takes on any value in the range $[0,2\pi]$ selected by a random number, r_ϕ , uniformly distributed in that range.

Both the θ and ϕ angles are calculated relative to the last direction in which the electron was moving before the impact. The direction θ_z^1 along which the electron is moving after the last deflection, relative to the z direction, is given by

$$\cos \theta_z^1 = \cos \theta_z \cos \theta + \sin \theta_z \sin \theta \cos \phi, \quad (26)$$

where θ_z is the angle relative to the z direction before the impact.

The motion Δz along the z direction is then calculated as

$$\Delta z = \Delta s \cdot \cos \theta_z^1. \quad (27)$$

The new angle θ_z^1 then becomes the incident angle θ_z for the next path length.

The initial energy of each secondary electron, produced by an inelastic collision, is calculated by

$$E_s = \Delta E + E_f, \quad (28)$$

where ΔE is now the total energy lost by the particle (positron) as calculated from the last inelastic collision, E_f is the Fermi energy [here included because ΔE is calculated from the dielectric excitation function (Ref. 21)]. The secondary electron trajectory is described exactly as the trajectory of the positrons of the primary beam, by including, of course, the appropriate cross sections. Note that the whole secondary electron cascade is followed in the numerical simulation.

Both positrons and secondary electrons are followed until their energy becomes lower than 16 eV (which for electrons corresponds to the Fermi energy plus the work function of the copper target, in the present case) with respect to the vacuum level. We assume that the secondary electrons are emitted with an angular distribution having spherical symmetry, as suggested by Shimizu and Ze-Jun.²¹

The surface energy barrier clearly influences the energy distribution of the ejected low-energy electrons. In particular, it should be noted that an electron cannot escape from the surface into vacuum with an angle θ higher than

$$\theta_c = \cos^{-1} \sqrt{\frac{(E_f + \varphi)}{(E + E_f + \varphi)}}, \quad (29)$$

where E_f is the Fermi energy and φ is the work function of the irradiated material (copper in the present case). Our numerical simulation may use both the classical and quantum-mechanical formula for the transmission coefficient. The data reported here used the quantum-mechanical formula.²¹ The number of positron trajectories simulated for each energy spectrum ranges from 10^4 to 10^6 and the overall cascade of the secondary electrons is followed in the computation.

V. RESULTS AND DISCUSSION

The results we are presenting have been obtained by the Monte Carlo procedure just described. The inelastic and elastic mean-free paths and the stopping powers we utilized are

TABLE I. Inelastic mean-free path and stopping power of electrons (Ashley *et al.*, 1976) and positrons (Ashley, 1990) in Cu.

$E - E_f$ (eV)	$\lambda_{inel}^{e^-}$ (Å)	$[-(dE/ds)]^{e^-}$ (eV/Å)	$\lambda_{inel}^{e^+}$ (Å)	$[-(dE/ds)]^{e^+}$ (eV/Å)
20	14.5	0.892		
30	6.48	3.10		
40	4.47	5.32	7.14	2.9
60	4.02	6.87	6.06	4.39
80	4.14	7.36	5.86	5.26
100	4.39	7.45	5.92	5.81
150	5.11	7.31	6.40	6.55
200	5.82	7.24	6.96	7.02
300	7.24	6.84	8.16	7.41
400	8.53	6.69	9.41	7.31
500			10.7	7.00
600	11.1	5.97	11.9	6.71
800	13.4	5.42	14.4	6.03
1000	15.6	5.27	16.9	5.44
1500			22.8	4.35
2000	26.1	3.80	28.4	3.64
4000	45.5	2.47	49.3	2.45
6000	63.5	1.86	68.7	1.88

TABLE II. Elastic mean-free path of electrons and positrons in Cu as a function of energy E . Our calculations.

E (eV)	$\lambda_{el}^{e^-}$ (Å)	$\lambda_{el}^{e^+}$ (Å)
20	1.56	3.98
25	2.27	4.12
30	2.85	4.24
40	3.66	4.46
50	4.14	4.66
60	4.40	4.84
70	4.53	5.02
80	4.6	5.19
90	4.65	5.35
100	4.69	5.51
150	4.91	6.21
200	5.22	6.80
250	5.59	7.33
300	5.97	7.81
400	6.75	8.68
500	7.47	9.45
600	8.15	10.2
700	8.78	10.8
800	9.38	11.4
900	9.94	12.0
1000	10.5	12.6
1500	12.9	15.1
2000	15.0	17.4
3000	18.8	21.4
4000	22.3	25.0
5000	25.6	28.5

TABLE III. Mean number, ν , of secondary electrons emitted per incident positron (of energy E_o).

E_o (eV)	ν
50	3.50
100	8.00
200	17.8
300	28.1
400	39.2
500	50.5
750	79.8
1000	110
1750	163
2000	233

summarized in Tables I and II. We evaluated that the accuracy of our calculation of the differential elastic scattering cross section is, for scattering angles higher than 5° , 1–2 % while that for the total elastic scattering cross section is of the order of 5–6 %. On the other hand the total cross section does not feature strongly in multiple-scattering processes: a systematic study of the first transport elastic scattering cross-section has shown that the accuracy of our approach is of the order of 2%.²³ Taking into account the inaccuracies in i) the elastic and inelastic cross-sections evaluation, ii) the approximations introduced by using the cubic spline interpolations of tabulated data, iii) the stopping power to calculate the energy losses, and iv) the statistical uncertainty of the Monte Carlo procedure, we are confident in concluding that our simulation give results with an accuracy within 5–15 %, ¹⁵ for electron and positron energies higher than ~ 100 eV. In the case of lower energies, we may anticipate larger inaccuracies because the evaluation of the cross sections is less accurate. In particular, in this low-energy regime (energies lower than 100–200 eV) the accuracy of the simulation should be evaluated by directly comparing the results with the available experimental data because it is well known that the theoretical evaluation of the relevant cross sections is still an open problem.

In Table III we report the mean number ν of secondary electrons emitted per incident positron as evaluated by the adopted Monte Carlo calculation. These mean numbers have been calculated by taking into account the whole electron

TABLE IV. Maximum range, R (Å), of positrons in Cu. E_o is the positron primary energy.

E_o (eV)	Mills and Willson ^a	Present MC calculation
200	–	95 ± 1
500	–	107 ± 2
1000	–	181 ± 3
2000	–	376 ± 3
3100	691	708 ± 7
4100	1035	1052 ± 7
5000	1246	1390 ± 10

^aReference 24.

TABLE V. Power index, m , and energy range where, by considering the calculated differential spectra of the energy distribution function of the secondary electrons emitted from a copper target, on a log-log (base 10) scale, we observed a linear trend (correlation coefficient, r , ≈ 0.99). E_{min} and E_{max} are the minimum and maximum energy of the selected energy range.

E_o (eV)	m	E_{min} (eV)	E_{max} (eV)	r
200	2.60	37.7	78.9	0.995
300	2.42	47.1	130	0.991
400	2.23	45.0	156	0.989
500	2.22	48.6	186	0.986
600	2.22	53.6	211	0.988
750	2.19	55.7	253	0.993
900	2.06	55.7	219	0.992
1000	1.95	60.7	189	0.993
1250	1.84	53.6	182	0.993
1500	1.75	53.6	153	0.987
1750	1.68	53.6	154	0.996
2000	1.59	46.4	146	0.996

cascade, which means that also the secondary electrons produced by the other secondary electrons are included in the calculation. As expected, ν increases with the positron primary energy.

In Table IV we report the maximum range, R , of the positrons in Cu as a function of the positron primary energy E_o . When possible we have compared the computed positron range with the experimental values obtained by Mills and Wilson.²⁴ The agreement is excellent for energies higher than 3000 eV. A comparison with the data reported in Fig. 5 of the quoted paper of Mills and Wilson showing positron transmission through Cu thin films suggests that, also for lower energies (1000 and 2000 eV), our evaluation of R is quite accurate (within 10%).

In Fig. 1 we report the $\Delta\rho/\Delta z$ ratio, which represents the calculated number of electrons emitted from the surface (divided by the total number of incident positrons), excited in the space interval $\Delta z (=0.43 \text{ \AA})$ around the space coordinate z , which emerge from the surface.

In Table V we report the Sickafus index m as calculated by performing a best linear fitting, over the energy range

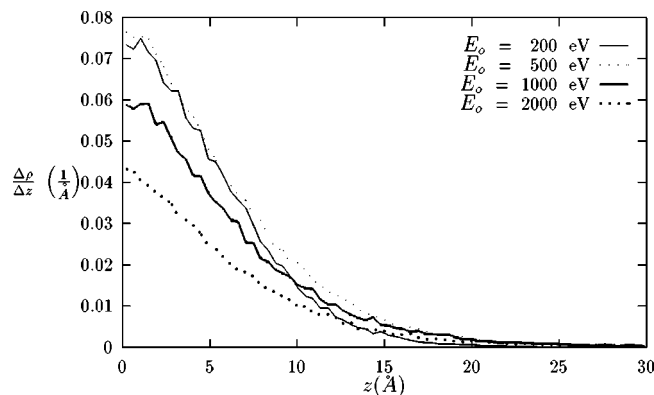


FIG. 1. Depth distribution $\Delta\rho/\Delta z$ of the secondary electrons emitted from the surface.

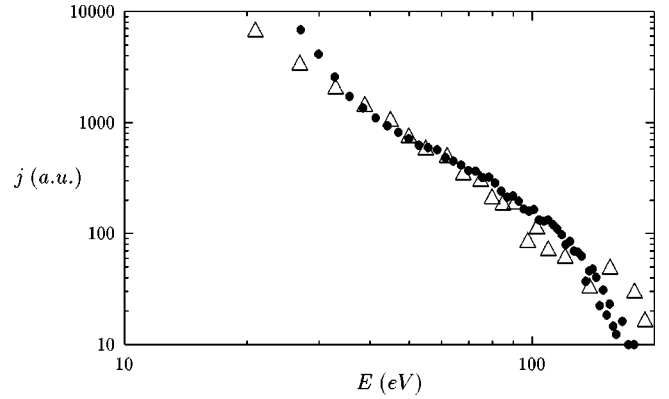


FIG. 2. Energy distribution of the secondary electrons ejected from copper stimulated by a positron beam of primary energy $E_o = 300$ eV. \triangle : Overton and Coleman experimental data (Ref. 4). \bullet : Present calculation.

specified in the same table, of the Monte Carlo simulation of the energy distribution of the secondary electrons ejected from Cu stimulated by positron beam having primary energies ranging from 200 eV to 2000 eV.

Our results concerning the differential spectra of the energy distribution function of the secondary electrons emitted from a copper target, above the low-energy cascade peak,⁴ always show, on a log-log (base 10) scale, a clear linear trend in agreement with both the Sickafus law [Eq. (1)]⁵⁻⁷ and Overton and Coleman⁴ experimental data (in the positron primary energy range from 200 eV to 2 keV). The calculation of the m coefficient of the Sickafus law [Eq. (1)] has been performed in the positron primary energy range from 200 eV to 2 keV at different incidence angle without observing any significant dependence on such a parameter. This is in agreement with the experimental results.⁴ In Figs. 2–4 we present our calculated energy spectra (full points) of the secondary electrons emitted following 300, 1000, and 2000 eV positron irradiation of copper, respectively: the comparison with the experimental data of Overton and Coleman (triangles)⁴ show a very good agreement. In Fig. 5, the numerical results for m , as a function of the incident positron energy, as well as the Overton and Coleman experimental data⁴ are reported. The incidence angle used in the calcula-

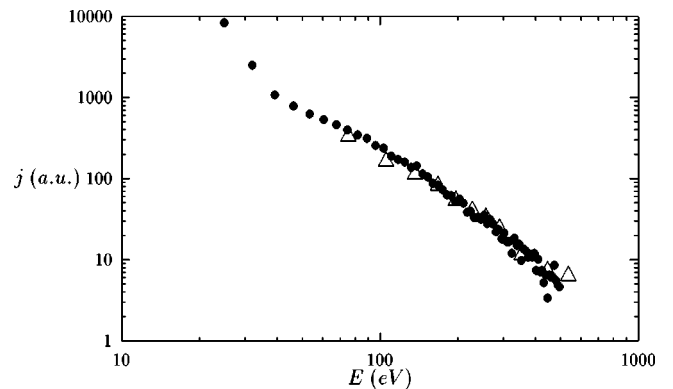


FIG. 3. Energy distribution of the secondary electrons ejected from copper stimulated by a positron beam of primary energy $E_o = 1000$ eV. \triangle : Overton and Coleman experimental data (Ref. 4). \bullet : Present calculation.

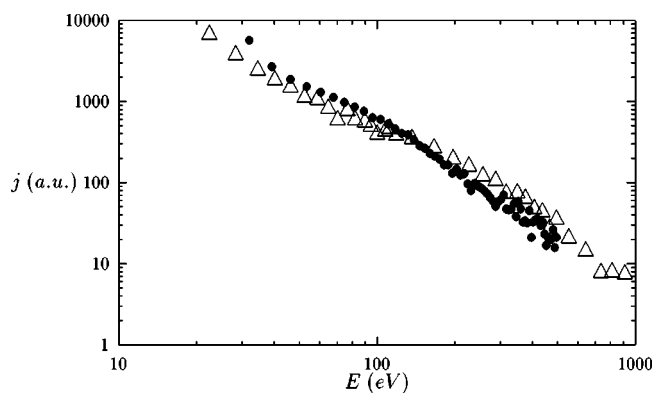


FIG. 4. Energy distribution of the secondary electrons ejected from copper stimulated by a positron beam of primary energy $E_o = 2000$ eV. Δ : Overton and Coleman experimental data (Ref. 4). \bullet : Present calculation.

tion was 35° with respect to the surface of the sample. The results show excellent agreement for positrons primary energies higher than ≈ 100 eV. However, when the positron primary energy is 100 eV or less, there is no agreement between theory and experiment. We attribute this discrepancy to the fact that the energy loss, in such a low-energy regime, cannot be regarded as continuous. To describe energy loss in such a low-energy regime, more appropriate calculations, as that performed with quantum Monte Carlo, are necessary.

Before concluding this section, a comment is appropriate to the qualitative argument reported by Overton and Coleman⁴ to try to justify the higher value of m when low-energy incident positrons are experimentally utilized. In particular, the authors suggest that this may be due to the fact that secondary electrons are generated at shallower depths beneath the surface and that, in this case, the probabilities for elastic and inelastic scattering before emerging into vacuum are quite low. If there are not any energy-loss collisions on the way to the exit surface then the theory of Mott²⁵ suggests a secondary electron energy spectrum to have the form E^{-2} . Note that the qualitative argument of Ref. 4 is quantitatively proved by the numerical results reported in our Fig. 1 where it is clearly shown that the emerging secondary electrons come from the first atomic layers beneath the surface.

VI. CONCLUSION

In conclusion, we have utilized the analytical Wolff's theory⁸ for secondary electron emission by showing that, for

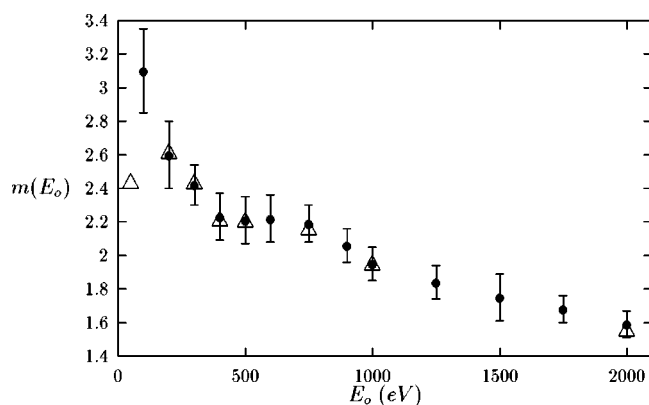


FIG. 5. Sickafus index m for secondary electrons ejected from copper by positrons as a function of the positron primary energy, E_o . Δ : Overton and Coleman experimental data (Ref. 4). \bullet : Present calculation including numerical errors due to statistical sampling.

energies exceeding ~ 100 eV, it may give m values not much different from the experimental ones. However this analytical approach is empirical because it extends Wolff's theory over energy region outside the suggested limits of validity of the same theory.

In order to avoid empirical analytical relations, we also used a numerical Monte Carlo procedure to make calculations in the positron primary energy range between 50 eV and 2 keV and for different incidence angles with respect to the surface of a copper sample. Many relevant numerical results have been obtained and reported, namely, (i) the elastic mean-free paths of positrons in copper, (ii) the mean number of electrons emitted per positron, (iii) the penetration depth of the positrons, and (iv) the depths from which the secondary electrons are emitted. Finally, the numerical results concerning the secondary electron energy distribution are compared with the experimental data recently presented by Overton and Coleman⁴ showing a general good agreement in a wide range of E values. In particular we have quantitatively explained the experimental data of the energy distribution of secondary electrons ejected from the surface of a copper target irradiated with a positron beam in the energy range from 200 eV to 2000 eV on the basis of all involved energy transfer mechanisms and by the statistics of the elastic scattering and slowing down of positrons and electrons in solids included in an appropriate Monte Carlo computational method.

¹A. Dupasquier and A. Zecca, Riv. Nuovo Cimento **8**, 1 (1985).

²P.J. Schultz and K.G. Lynn, Rev. Mod. Phys. **60**, 701 (1988).

³P. Asoka-Kumar, K.G. Lynn, and D.O. Welch, J. Appl. Phys. **76**, 4935 (1994).

⁴N. Overton and P.G. Coleman, Phys. Rev. Lett. **79**, 305 (1997).

⁵E.N. Sickafus, Phys. Rev. B **16**, 1436 (1977).

⁶E.N. Sickafus, Phys. Rev. B **16**, 1448 (1977).

⁷E.N. Sickafus and C. Kukla, Phys. Rev. B **19**, 4056 (1979).

⁸P.A. Wolff, Phys. Rev. **95**, 56 (1954).

⁹M.L. Goldberger, Phys. Rev. **74**, 1269 (1948).

¹⁰C.J. Powell, J. Vac. Sci. Technol. **13**, 219 (1976).

¹¹J.C. Ashley, C.J. Tung, R.H. Ritchie, and V.E. Anderson, IEEE Trans. Nucl. Sci. **NS23**, 1833 (1976).

¹²J.C. Ashley, J. Electron Spectrosc. Relat. Phenom. **46**, 199 (1988).

¹³J.C. Ashley, J. Electron Spectrosc. Relat. Phenom. **50**, 323 (1990).

¹⁴M. Dapor, Phys. Rev. B **46**, 618 (1992).

¹⁵M. Dapor and A. Miotello, Eur. Phys. J.: Appl. Phys. **5**, 143 (1999).

- ¹⁶J. Barò, J. Sempau, J.M. Fernández Varea, and F. Salvat, Nucl. Instrum. Methods Phys. Res. B **100**, 31 (1995).
- ¹⁷A. Miotello and M. Dapor, Phys. Rev. B **56**, 2241 (1997).
- ¹⁸A. Dubus, J.C. Dehaes, J.P. Ganachaud, A. Hafni, and M. Cailler, Phys. Rev. B **47**, 11 056 (1993).
- ¹⁹K. Ohya, Jpn. J. Appl. Phys., Part 1 **33**, 4735 (1994).
- ²⁰S. Ichimura, R. Shimizu, and Ding Ze-Jun, Surf. Interface Anal. **13**, 149 (1988).
- ²¹R. Shimizu and Ding Ze-Jun, Rep. Prog. Phys. **55**, 487 (1992).
- ²²M. Dapor, J. Appl. Phys. **79**, 8406 (1996).
- ²³M. Dapor and A. Miotello, At. Data Nucl. Data Tables **69**, 1 (1998).
- ²⁴A.P. Mills and R.J. Wilson, Phys. Rev. A **26**, 490 (1982).
- ²⁵N.F. Mott, Proc. R. Soc. London, Ser. A **126**, 259 (1930).